

Discovery of a radio nebula around PSR J0855–4644

C. Maitra¹★, S. Roy², F. Acero³, Y. Gupta²

¹Max-Planck-Institut für extraterrestrische Physik, Giessenbachstraße, 85748 Garching, Germany

²National Centre for Radio Astrophysics, TIFR, Pune University Campus, Post Bag 3, Pune 411 007, India

³Laboratoire AIM, CEA/DRF - CNRS - Université Paris Diderot, IRFU/DAP, CEA-Saclay, 91191 Gif-sur-Yvette, France

Accepted.....; Received

ABSTRACT

We report the discovery of a diffuse radio emission around PSR J0855–4644 using an upgraded *GMRT* (*uGMRT*) observation at 1.35 GHz. The radio emission is spatially coincident with the diffuse X-ray pulsar wind nebula (PWN) seen with *XMM-Newton* but is much larger in extent compared to the compact axisymmetric PWN seen with *Chandra*. The morphology of the emission, with a bright partial ring-like structure and two faint tail-like features strongly resembles a bow shock nebula, and indicates a velocity of 100 km/s through the ambient medium. We conclude that the emission is most likely to be associated with the radio PWN of PSR J0855–4644. From the integrated flux density, we estimate the energetics of the PWN.

Key words: stars: pulsars: PSR J0855–4644; radio continuum: ISM

1 INTRODUCTION

Young rotational powered pulsars are the powerhouses of pulsar wind nebulae (PWNe from now). Rotational powered pulsars lose a significant part of their energy via relativistic winds which, upon interactions with the ambient medium, produce a synchrotron powered nebula emitting from radio to beyond the X-ray bands. The integrated energy spectrum is of synchrotron type, with a power-law having a spectral break around 10^{13} – 10^{15} Hz. In the radio band, the spectrum is expected to be flat, $F_\nu \propto \nu^{-\alpha}$, with α between 0 and 0.3, while α is > 1 in the X-ray band. The steepening of the spectrum in X-rays, and hence the spectral break is most commonly associated with losses due to synchrotron cooling. Furthermore, in the radio band the PWN luminosity traces the integrated history of the pulsar spin-down, while in X-rays the PWN luminosity traces the current energy output of the central pulsar (Reynolds & Chevalier 1984). The PWN morphology provides crucial information on the properties of the outflow, the interacting ambient medium and also the geometry of the pulsar powering it (Reynolds et al. 2017).

PSR J0855–46444 is a young and energetic pulsar discovered by the Parkes multibeam radio survey (Kramer et al. 2003). It lies in the Vela region ($l \approx 265^\circ$, $b \approx -1^\circ$) which is a complex region in the sky with many overlapping supernova remnants (SNRs) along our line of sight. Especially worth mentioning is the Vela remnant, one of the brightest and most extended remnants in the sky (Duncan et al. 1996). Having a large angular size of 8° diameter, it overlaps several SNRs such as Puppis A and RX J0852.0–4622. PSR J0855–4644 is located on the south-eastern rim of RX J0852.0–4622 *aka* the Vela Jr, but is not associated with it. The

measured spin period (P) of 65 ms and the period derivative (\dot{P}) of $7.3 \times 10^{-15} \text{ s s}^{-1}$ result in a spin-down luminosity (\dot{E}) of 1.1×10^{36} erg/s (assuming a moment of inertia (I) of 10^{45} g cm^2 for standard neutron star parameters). The characteristic age ($\tau_c \equiv P/2\dot{P}$) is estimated to be 140 kyr.

The source was observed with *XMM-Newton*, which revealed the X-ray counterpart of the pulsar surrounded by a diffuse non-thermal extended emission which is the PWN associated with it (Acero et al. 2013). Additionally, comparison of column densities provided an upper limit of 900 pc for the distance to the source. A dedicated *Chandra* observation revealed a further compact X-ray nebula with an axisymmetric morphology resembling a double torus PWN, analogous to the Vela PWN which has an \dot{E} similar to PSR J0855–4644 (Maitra et al. 2017). However, this nearby energetic PWN has not been reported to be followed up in the radio wavelengths so far.

In this letter we report the discovery of the radio counterpart of the PWN surrounding PSR J0855–4644 using an observation with the upgraded *GMRT* (*uGMRT*) (Gupta et al. 2017). Sect. 2 presents the observations and analysis, Sect. 3 the results, Sect. 4 the discussion on the nature of the radio emission and the inferred properties. Finally Sect. 5 presents the summary and conclusions.

2 OBSERVATION & ANALYSIS

Observations with the *uGMRT* were carried out on 30 January 2017 for 6 hours. All 30 antennas of the array were used to obtain maximum u – v coverage. The pointing centre was RA: $08^{\text{h}}55^{\text{m}}36.0^{\text{s}}$ and DEC: $-46^{\text{h}}44^{\text{m}}13.2^{\text{s}}$. Observations were carried out at 1.35 GHz with a bandwidth of 200 MHz using 1024 spectral channels. 3C147

★ Contact e-mail: cmaitra@mpe.mpg.de

was used as primary flux density and bandpass calibrator. The VLA calibrator 0835-451¹ was observed as a secondary calibrator. This calibrator was observed every 30 minutes. After calibration and editing, frequency channels were averaged by a factor of 8 to provide a channel width of 1.56 MHz in the output data. This process significantly reduced the data volume while keeping bandwidth smearing smaller than the synthesized beam during imaging up to half power point of the antennas. The initial images were improved by phase-only calibration and at the last stage by an amplitude and phase self-calibration. The data were then used to image the target source with a short UV cutoff of 0.7 kilo-lambda which resolved out extended structures of angular size $\gtrsim 2.5'$ in the field. The imaging methodology used in the current work could have missed a possible large scale structure of size $\gtrsim 4'$. To verify this we made another image with a lower UV cutoff as set by the data to 200 lambda. No other significant emission brighter than 2σ or $\sim 110 \mu\text{Jy/beam}$ (beam size $9'' \times 5''$) was seen around the emission.

3 RESULTS

Fig. 1 (right) shows the 1.35 GHz *uGMRT* image of the region around PSR J0855-4644 showing the diffuse structure around the pulsar. The integrated flux density of the radio emission is 14 ± 2 mJy, and the significance of the emission is 7σ . Enhanced emission is also detected at the position of the pulsar at a flux density of ~ 0.5 mJy. This is consistent with the estimated flux of the pulsar at 1.4 GHz from Kramer et al. (2003). We find the position of the pulsar to be at RA: $08^{\text{h}}55^{\text{m}}36.29^{\text{s}} \pm 0.02^{\text{s}}$ and DEC: $-46^{\text{h}}44^{\text{m}}15.29^{\text{s}} \pm 0.42^{\text{s}}$. The difference in RA between the originally reported radio position and the present one is $\sim 1.5''$. This could arise due to the proper motion of the pulsar in the sky plane. This is however unlikely because the position of the pulsar reported in radio (Kramer et al. 2003, 1999) and in X-rays (Maitra et al. 2017, 2012) at different epochs are consistent with each other. In the absence of any known high resolution ($\sim 1''$) and high sensitivity observation of the field near 1.4 GHz, we cannot check the positions of other background sources in the *GMRT* 1.35 GHz field of view. Field sources observed at 1.35 GHz could be systematically offset (by $\sim 1.5''$) due to the phase change caused by ionospheric effects between the target field and the phase calibrator.

Fig. 1 (left) shows a Red-Blue image of the region with the 1.35 GHz *uGMRT* image in red and the 0.5–8 keV *Chandra* image from Maitra et al. (2017) in blue. The white contours denote the 3, 4 and 5σ contours of the diffuse X-ray PWN from Acero et al. (2013). The extent of the radio feature is much larger than the compact axisymmetric nebula seen with *Chandra*, and is comparable to the diffuse X-ray nebula seen with *XMM-Newton*. The central ring-like radio emission surrounding the pulsar is $\sim 45''$ in diameter, and is of the same size as the inner nebula seen with *XMM-Newton*. This corresponds to the innermost white contour denoting the emission at 5σ significance. A brightening is observed at the south-eastern region of the ring. Two extended tail-like features extend in the north-west direction making the total nebula about $1.5'$ ($90''$) in extent. It is worth noting that Acero et al. (2013) reported diffuse X-ray emission up to $\sim 150''$. However, as can be seen from the over-plotted contours, the 3σ emission extends only up to $90''$. Further the X-ray emission seen with *XMM-Newton* is

contaminated with the Vela SNR at energies < 1 keV, and by the non-thermal emission from the Vela Jr at energies > 1 keV. Therefore, any low significance emission should be treated with caution.

4 DISCUSSION

At the estimated distance of 900 pc, the radio nebula detected around PSR J0855-4644 corresponds to a physical size of 0.44 pc. The inferences on the nature of the radio emission and some derived physical properties of the system are given below.

4.1 Nature of the radio emission

The spatial coincidence of the enhanced radio emission with the diffuse X-ray emission surrounding PSR J0855-4644, is a strong indication that we have discovered the radio counterpart of the PWN. However, in the absence of radio data at two different wavelengths, the spectral index of the source cannot be determined which would establish the nature of the emission as non-thermal with certainty (as is expected from PWNs). In the absence of this, we have investigated the possibility of this emission emerging from two other competing phenomena: a SNR associated with PSR J0855-4644 and an overlapping HII region.

First we assume that the ring-like radio structure surrounding the pulsar is an associated SNR. In this hypothesis, we can fix a lower limit for the age of the SNR to 10 kyr (the characteristic age of the PSR is 140 kyr but this estimate is often an overestimate of the true age of the system). At a distance of 900 pc, the physical radius is 0.1 pc. The Sedov-Taylor equation relates the radius of the forward shock (R_{sh}) as a function of time (t) for a given supernova explosion energy (E), and density (n_0) as:

$$R_{\text{sh}} = 5.06 \left(\frac{n_0}{1 \text{ cm}^{-3}} \right)^{1/5} \left(\frac{E}{10^{51} \text{ ergs}} \right)^{1/5} \left(\frac{t}{10^3 \text{ years}} \right)^{2/5} \text{ pc} \quad (1)$$

Assuming $E = 10^{51}$ ergs, n_0 is $\sim 10^{10} \text{ cm}^{-3}$ (for $R_{\text{sh}} = 0.1$ pc and age $t=10$ kyr). In the unlikely scenario where the pulsar distance is overestimated by a factor of 10 (i.e. $R_{\text{sh}} = 1$ pc), n_0 would be still be very high (10^5 cm^{-3}). Assuming a cloud of size similar to the partial shell-like source with a density of 10^{10} cm^{-3} (10^5 cm^{-3}), its associated column density (N_{H}) would be $6 \times 10^{27} \text{ cm}^{-2}$ ($6 \times 10^{22} \text{ cm}^{-2}$). Comparing this from the HI and ^{12}CO data along the line of sight to the pulsar (Fig. 6 of Acero et al. 2013), $N_{\text{H}} \sim 1.5 \times 10^{22} \text{ cm}^{-2}$, when integrated over all velocities. Therefore, we conclude that the association of the ring-like structure with a SNR evolving in a dense molecular cloud is unlikely.

We also consider the possibility of the emission being thermal free-free in nature. This region has been observed by the *WISE* survey at $22 \mu\text{m}$ (Wright et al. 2010). Infra-red emission at $24 \mu\text{m}$ has earlier been shown to be highly correlated with Paschen- α emission (Calzetti et al. 2005) and is used as a proxy of thermal emission (Murphy et al. 2006) from galaxies. Emission at this band can be used to predict the thermal emission in the radio band (Basu & Roy 2013). Dust emissivity at a very nearby wavelength of $22 \mu\text{m}$ is expected to be quite close to its $24 \mu\text{m}$ emission and can be used as a tracer of HII region density. The Model by Gordon et al. (2017) indicate the dust emission at $24 \mu\text{m}$ to be $\sim 15\%$ higher than what is measured at $22 \mu\text{m}$ from *WISE* data. From the background subtracted images, we did not detect any emission at the position of the source from the *WISE* map at $22 \mu\text{m}$ (Fig. 2). The measured upper limit of its flux density at $22 \mu\text{m}$ is 700 DN (*WISE* map unit). Using

¹ <https://science.nrao.edu/facilities/vla/observing/callist>

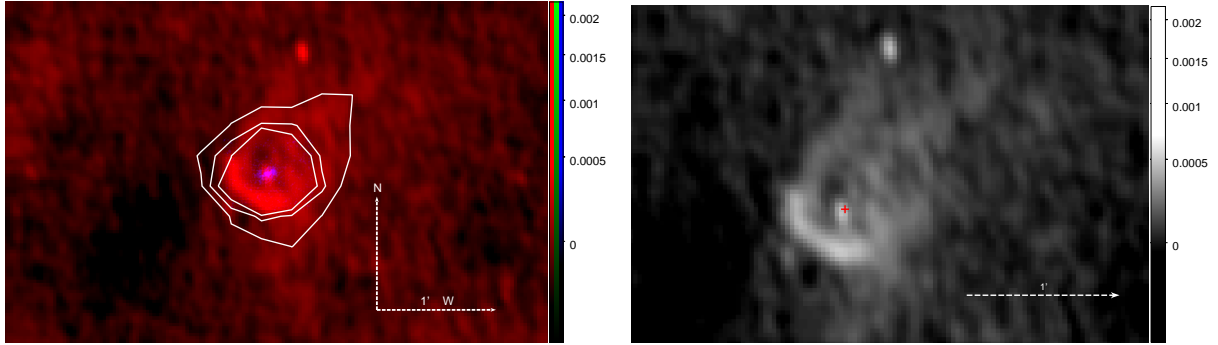


Figure 1. *Left:* Red-Blue image of the region. Red: 1.35 GHz *uGMRT* image of the region around PSR J0855–4644 showing diffuse emission around the pulsar. Resolution of the radio image is $9'' \times 5''$. Its major and minor axis is $9''$ and $5''$ respectively and the beam position angle is 16° (major axis orientation from North towards East). Blue: 0.5–8 keV *Chandra* image showing the compact PWN. The solid white contours denote the 3, 4 and 5σ contour around the diffuse X-ray PWN detected with *XMM-Newton* (1.2–6 keV). *Right:* A zoomed in view showing the radio nebula and the shell structure. The red cross marks the position of the pulsar as reported in Kramer et al. 2003.

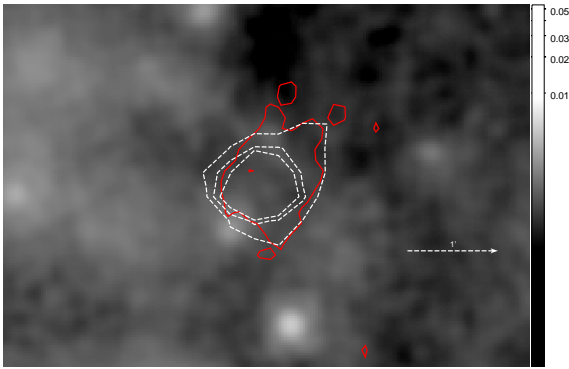


Figure 2. $22\ \mu\text{m}$ *WISE* background subtracted image of the region around PSR J0855–4644. Resolution of the image is $12''$. The dashed white contours denote the *XMM-Newton* contours in Fig. 1. The solid red contours denote radio contour at the level of 1 mJy/beam.

the conversion of DN to Jy (5.22×10^{-5})², and using the expected conversion from $22\ \mu\text{m}$ to $24\ \mu\text{m}$ as described above, the upper limit of the $24\ \mu\text{m}$ flux density from the region is 0.04 Jy. We assume the electron temperature of any thermal gas in the region to be 10^4 K. Following Basu & Roy (2013), the predicted upper limit of thermal emission at 1.35 GHz from the region is 0.3 mJy. This is almost 2 orders of magnitude lower than what is measured at 1.35 GHz from our observation. As noted in Basu & Roy (2013), the conversion of $24\ \mu\text{m}$ emission to radio band could be uncertain typically by up to a factor of 2. Therefore, we conclude that the emission from the region seen in radio cannot be free-free emission in nature.

Having ruled out the above two scenarios, we infer that the radio emission is most likely to be associated with the PWN. The morphology of the emission, with a bright partial ring-like structure in the south-east and two faint tail-like features in the north-west direction is reminiscent of a bow shock nebula. The direction of the westernmost tail is somewhat aligned along the spin axis of the pulsar derived in Maitra et al. (2017) (offset by $\sim 10^\circ$). This is in further support of its bow shock origin. Bow shock nebulae are formed when a pulsar moves supersonically through the ambient medium. They are most often seen either in non-recycled pulsars with ages between 10 kyr and 3 Myr, or in older recy-

cled pulsars. The observed spin-down luminosities (\dot{E}) range from $10^{33} - 10^{37}$ erg/s (Kargaltsev et al. 2017, and references therein). A faint bow shock nebular structure in the radio band has also been detected in the Vela pulsar; a system analogous to PSR J0855–4644 (Chevalier & Reynolds 2011). Although the proper motion for PSR J0855–4644 is not yet known, the bow shock structure indicates supersonic motion through the local medium. In this case the termination shock radius (R_{Ts}) can be determined from the balance between the relativistic wind of the pulsar and the ram pressure at the head of the shock. This is expressed as (Cheng et al. 2004)

$$R_{Ts} \sim 3 \times 10^{16} \dot{E}_{34}^{\frac{1}{2}} n_1^{-\frac{1}{2}} v_{p,100}^{-1} \text{ cm}. \quad (2)$$

Here n_1 is the number density in units of particles cm^{-3} and $v_{p,100}$ is the space velocity of the pulsar in units of 100 km/s. Assuming the partial-ring to be the termination surface R_{Ts} , the distance between the pulsar and the tip of the bow shock is $\sim 20''$ (~ 0.1 pc at a distance of 900 pc). Given an \dot{E} of 10^{36} erg/s and a typical ambient density of $1\ \text{cm}^{-3}$, the velocity of the pulsar is ~ 100 km/s. Further assuming that the transverse velocity of the pulsar is comparable to the velocity estimated as above, a shift of $\sim 0.5''$ is expected between the radio and the X-ray observation separated by 13 years. Given the uncertainty in the determination of the positions, such a shift would not be noticeable and is consistent with our results. Future deeper and more sensitive observations separated by a large time gap will ascertain this.

4.2 Comparison between the radio and X-ray emission

The difference between the size of the radio and X-ray PWN mainly depends on whether synchrotron cooling has set in. This can often lead to a difference in size between the radio and X-ray PWN. Since the higher energy X-ray electrons cool faster, the number of X-ray emitting particles decrease rapidly with increasing distance from the pulsar leading to a smaller size of the X-ray nebula compared to the radio counterpart. For the same reason a steepening in the power-law spectral index of the synchrotron emission is also observed frequently. The break frequency ν_{break} is a function of the age of the pulsar and the magnetic field of the nebula, i.e. lower values of ν_{break} are expected for higher nebular magnetic fields B_{neb} . Therefore systems which have comparable sizes of the X-ray and radio nebula have either weak B_{neb} or are intrinsically young PWNe where the process of cooling has not yet set in (e.g. 3C 58, G130.7+3.1: Gaensler & Slane 2006). Furthermore,

² http://wise2.ipac.caltech.edu/docs/release/allsky/expsup/sec2_3f.html

the radio and the X-ray emission are not always spatially correlated and even anti-correlation has been observed, e.g., for Vela (Dodson et al. 2003); and G319.9-0.97 (Ng et al. 2010).

Comparison between the radio and X-ray emission around PSR J0855–4644 (Fig. 1) indicates that the radio nebula is comparable in size with the X-ray nebula. The faint tail-like features of the radio emission in the north-west however extend beyond the X-ray emission. This indicates that the size of the X-ray PWN \leq to the radio counterpart. The \dot{E} and the morphology of the compact X-ray PWN around PSR J0855–4644 point to a Vela-like pulsar, generally categorized as fast-spinning pulsars with characteristic ages $10 \text{ kyr} \lesssim \tau_c \lesssim 100 \text{ kyr}$ and $\dot{E} \gtrsim 10^{36} \text{ erg/s}$ (Kramer et al. 2003). Although the characteristic age of the system is measured to be 140 kyr, it is to be noted that this is often an overestimation of the age of the system (e.g. Migliazzo et al. 2002). Therefore PSR J0855–4644 is not a young PWN (Crab-like) where synchrotron cooling might not have set in. This indicates that the system has a weak B_{neb} which renders the cooling time-scales to be longer.

4.3 Inferred properties of the system

From the integrated flux density, the radio luminosity of the PWN (L_R) can be estimated assuming a typical spectral index of -0.3 between 10^7 and 10^{11} Hz , and using equation (4) in Frail & Scharringhausen (1997). The estimated L_R is $\sim 1.3 \times 10^{30} \text{ erg/s}$ and the radio efficiency $L_R/\dot{E} \equiv \eta_R$ is $\sim 1 \times 10^{-6}$. Given that the flux is measured only at one frequency and not integrated over the entire frequency range of emission of the radio nebula, this is a lower limit. Both L_R and η_R are however very similar to that obtained for the Vela pulsar (Dodson et al. 2003).

5 SUMMARY

From radio observations using the *uGMRT* at 1.35 GHz, we have discovered diffuse radio emission surrounding the Vela-like pulsar PSR J0855–4644, for the first time. A central ring-like radio emission feature surrounds the pulsar, which is brightened at the south-east region. Two tail-like features extend in the north-west direction. A faint diffuse emission fills the whole feature. The structure corresponds to a physical size of 0.44 pc. This is much larger than the compact axisymmetric X-ray nebula (0.06 pc) seen with *Chandra* but is similar in extent to the diffuse X-ray nebula seen with *XMM-Newton*.

The spatial coincidence of the radio emission with the diffuse X-ray emission is in strong favour of it being the radio counterpart of the PWN. We have also ruled out its origin as an overlapping SNR on a HII region along the line of sight, given the size of the structure, its comparison with HI and ^{12}CO data along the line of sight to the pulsar, and the *WISE* infrared maps. The PWN morphology strongly resembles a bow shock nebula and the radius of the termination shock indicates a velocity of 100 km/s through the ambient medium.

The integrated flux density at 1.35 GHz provides an estimate of $L_R \sim 1.3 \times 10^{30} \text{ erg/s}$ and $\eta_R \sim 1 \times 10^{-6}$. These are similar to that observed in the Vela PWN.

ACKNOWLEDGMENTS

We thank the referee for providing very useful comments which helped to improve the paper. We thank the staff of the *GMRT* that

made these observations possible. *GMRT* is run by the National Centre for Radio Astrophysics of the Tata Institute of Fundamental Research.

REFERENCES

- Acero F., Gallant Y., Ballet J., Renaud M., Terrier R., 2013, *A&A*, **551**, A7
 Basu A., Roy S., 2013, *MNRAS*, **433**, 1675
 Calzetti D., et al., 2005, *ApJ*, **633**, 871
 Cheng K. S., Taam R. E., Wang W., 2004, *ApJ*, **617**, 480
 Chevalier R. A., Reynolds S. P., 2011, *ApJ*, **740**, L26
 Dodson R., Lewis D., McConnell D., Deshpande A. A., 2003, *MNRAS*, **343**, 116
 Duncan A. R., Stewart R. T., Haynes R. F., Jones K. L., 1996, *MNRAS*, **280**, 252
 Frail D. A., Scharringhausen B. R., 1997, *ApJ*, **480**, 364
 Gaensler B. M., Slane P. O., 2006, *ARA&A*, **44**, 17
 Gordon K. D., et al., 2017, *A&A*, **603**, A114
 Y. Gupta , B. Ajithkumar , H. S. Kale , S. Nayak , S. Sabhapathy , S. Sureshkumar , R. V. Swami , J. N. Chengalur , S. K. Ghosh , C. H. Ishwara-Chandra , B. C. Joshi , N. Kanekar , D. V. Lal , S. Roy 2017, *Current Science*, **113**, 707
 Kargaltsev O., Pavlov G. G., Klingler N., Rangelov B., 2017, *Journal of Plasma Physics*, **83**, 635830501
 Kramer M., et al., 2003, *MNRAS*, **342**, 1299
 Maitra C., Acero F., Venter C., 2017, *A&A*, **597**, A75
 Migliazzo J. M., Gaensler B. M., Backer D. C., Stappers B. W., van der Swaluw E., Strom R. G., 2002, *ApJ*, **567**, L141
 Murphy E. J., et al., 2006, *ApJ*, **638**, 157
 Ng C.-Y., Gaensler B. M., Chatterjee S., Johnston S., 2010, *ApJ*, **712**, 596
 Reynolds S. P., Chevalier R. A., 1984, *ApJ*, **278**, 630
 Reynolds S. P., Pavlov G. G., Kargaltsev O., Klingler N., Renaud M., Mereghetti S., 2017, *Space Sci. Rev.*, **207**, 175
 Wright E. L., et al., 2010, *AJ*, **140**, 1868